NANO LETTERS

pubs.acs.org/NanoLett

Nanostructured LaB_6 Field Emitter with Lowest Apical Work Function

Han Zhang,[†] Jie Tang,*[,†] Jinshi Yuan,[†] Jun Ma,[†] Norio Shinya,[†] Kiyomi Nakajima,[†] Hideyuki Murakami,[†] Tadakatsu Ohkubo,[†] and Lu-Chang Qin*[,‡]

[†]National Institute for Materials Science, Tsukuba 305-0042, Japan, and [‡]Department of Physics and Astronomy, Curriculum in Applied Sciences and Engineering, University of North Carolina at Chapel Hill, Chapel Hill, North Carolina 27599-3255

ABSTRACT LaB_6 nanowires are ideal for applications as an electrical field-induced ion and electron point source due to their miniature dimensions, low work function, as well as excellent electrical, thermal, and mechanical properties. We present here a reliable method to fabricate and assemble single LaB_6 nanowire-based field emitters of different crystal orientations. The atomic arrangement, emission brightness from each crystal plane, and field emission stability have been characterized using field ion microscopy (FIM) and field emission microscopy (FEM). It is found that the ⟨001⟩ oriented LaB_6 nanowire emitter has the highest field emission symmetry while the ⟨012⟩ oriented LaB_6 nanowire has the lowest apical work function. The field emission stability from the single LaB_6 nanowire emitter is significantly better than either the LaB_6 needle-type emitter or W cold field emitters.

KEYWORDS Electron emission, nanowire, lanthanum hexaboride, field emission, field ion miscroscopy, field emission microscopy

As a fundamental tool in research ranging from materials science to biology, the electron microscope, including both the transmission electron microscope (TEM) and the scanning electron microscope (SEM), has been achieving an ever higher spatial, temporal, and energy resolution. This requires the point electron source of the electron microscope to generate a brighter, more temporally coherent and more stable electron beam for illumination. A cold field emitter (CFE) offers the highest brightness and temporal coherence over other types of electron sources, such as the Schottky emitter and the thermionic emitter.[1] For a CFE, the source brightness is associated with the emission current density, which can be described by the simplified Fowler−Nordheim equation in the form of the following equation[2,3]

$$J = c_1 \frac{F^2}{\phi} \exp\left(-c_2 \frac{\phi^{\frac{3}{2}}}{F}\right) \quad (1)$$

where the variables F and ϕ are the local electric field strength and the emitter material work function, respectively, while c_1 and c_2 can be treated as constants under practical operational conditions. The temporal coherence of a CFE, characterized by the energy spread of the emitter, can be presented as

$$\Delta E = c_3 F/\sqrt{\phi} \quad (2)$$

with c_3 being a constant.[4] Therefore, the emission current density can be regarded as a function of the two independent variables ϕ and ΔE after combining eqs 1 and 2

$$J = c_4 \Delta E^2 \exp\left(-c_5 \frac{\phi}{\Delta E}\right) \quad (3)$$

where c_4 and c_5 are combined coefficients. From eq 3, we can calculate that a CFE with a lower work function will offer both a higher emission current density and a lower energy spread.[5] On the other hand, during the process of field-induced emission, ion bombardment from the residual gases leads to emission current fluctuations and local arcing, which often damage the emitter tip.[6,7] One solution to this problem is to use an emitter material of higher hardness to resist ion bombardment. Because of the above considerations, LaB_6 has long been regarded as an ideal field emitter material.[8−10] Compared with the conventional W CFE, LaB_6 has a work function below 2.5 eV, much lower than that of the work function of W which is 4.5 eV.[11−14] In addition, the hardness of LaB_6 is 5−10 times higher than that of W, therefore promises an improved resistance against ion bombardment.[15−17] LaB_6 also has high conductivity, high melting point, and is chemically stable and therefore promises to make a practical field ion and field electron emitter. The research about using LaB_6 as field emitter material has been a continuing effort ever since 1960s.[18−22] To make a LaB_6 field emission point source, a LaB_6 single crystal was usually prepared by floating zone refinement, carefully cut into a

* To whom correspondence should be addressed.
Received for review: 05/18/2010
Published on Web: 08/17/2010

DOI: 10.1021/nl101752z | *Nano Lett.* **2010,** *10,* 3539–3544

thin rod (~200 μm in diameter), and then etched electrochemically to form a needle with a conical tip (~100 nm in radius of curvature).[23,24] Before field electron emission, high-temperature flashing (~1500 °C) was usually applied to eliminate surface contaminants to clean the LaB_6 surface. However, it was found difficult to control the LaB_6 surface morphology, chemical composition, and stoichiometry during the process of thermal-flashing and no stable cold-field electron emission has been observed. On the other hand, field evaporation is an alternative to clean a field emitter surface.[25] It is a cold process which desorbs the contamination layer off the emitter surface through ionization. The emitter surface cleaned by field evaporation maintains its original chemical composition and stoichiometry and has a predictable tip geometry. However, for an emitter with a conical tip, field evaporation dulls the emitter tip by increasing its tip radius of curvature. Consequently, the extraction voltage needs to be increased every time when field evaporation is performed to keep the initial emission current density. For this reason, field evaporation, although proven to be an effective means for surface cleaning in the field of surface science and atom probe microscopy, cannot be used for a conical field electron emitter in practical operations where repetitive cleaning is often necessary.

Such field evaporation-induced tip dulling can be avoided if LaB_6 nanowires are used as a field emitter. The LaB_6 nanowires naturally bear a nanometric sharp tip (can be smaller than 10 nm in diameter) and are therefore suitable for being used as a field emitter without the need for any additional sharpening process. Its large aspect ratio and uniform diameter ensure that the tip radius of curvature always stays the same even when field evaporation is performed in a repetitive manner. On top of that, the versatility in controlling the crystallographic orientation of LaB_6 nanowires also enables us to engineer a nanostructured LaB_6 CFE with desired apex symmetry and work function.[26,27] To demonstrate this possibility, we have developed a reliable approach to fabricate nanostructured LaB_6 CFEs and fabricated a ⟨001⟩ oriented LaB_6 nanowire emitter with a highly symmetric field emission pattern and a ⟨210⟩ oriented LaB_6 nanowire emitter with the lowest apical work function. The H_2 gaseous ion emission and field-induced electron emission have both been directly characterized using field ion microscopy (FIM) and field emission microscopy (FEM).[28] The electric field-induced electron emission from a clean surface of the LaB_6 nanowire has no decay after surface cleaning. This is in contrast with the large emission current decay (>90%) for W CFEs.[29]

The work presented herein is based on earlier preliminary investigations on the synthesis and field electron emission of LaB_6 nanostructures.[27,30−32] A single LaB_6 nanowire is picked up from substrate using an in-house developed nanomanipulation system with which the nanowire is aligned to the desired direction. The fabrication process of the nanowire emitter is highly reliable and reproducible. The

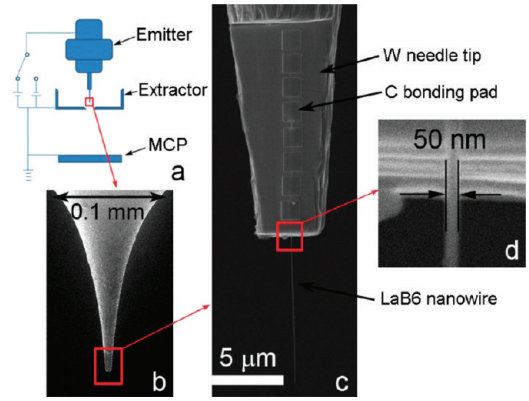

FIGURE 1. Experimental setup and structure of LaB_6 single nanowire CFE. (a) Schematic of FIM/FEM setup and the location of LaB_6 nanowire in the emitter is indicated. (b) A magnified view of the W needle tip where the LaB_6 nanowire is bonded to a flat fabricated at the tip of the W needle by FIB. (c) Top view of the emitter tip showing its constituting parts of W flat, C bonding pads, and LaB_6 nanowire. (d) Magnified view of the section of the LaB_6 nanowire near the edge of the W flat.

experimental setup is shown schematically in Figure 1a. The emitter consists of a stainless steel holder that holds a free-standing W needle. An extractor is placed about 2 mm in front of the W needle tip. A high voltage of switchable polarity is applied between the emitter and the extractor for the FIM or FEM operations. A microchannel plate (MCP) and phosphorus screen system is placed behind the extractor to visualize the emitted charged particles. Figure 1b is an SEM image of the W needle tip formed by electrochemical etching. A magnified view shows that a single LaB_6 nanowire has been fixed on the top of a flat fabricated on the tip of the W needle, as shown in Figure 1c. A portion of the nanowire, about 10 μm in length, extends out of the W flat as the emitting element. Eight carbon micropads are fabricated using electron beam-induced deposition to bond the LaB_6 nanowire to the W flat to ensure strong binding and high electrical conductance. Figure 1d is a magnified SEM image showing the joint of the LaB_6 nanowire and the W tip, revealing its diameter of around 50 nm. The single nanowire emitter has also been examined in side-view to confirm its parallel alignment with the W needle axis.

The as-synthesized ⟨001⟩ oriented LaB_6 nanowire usually has a square cross-section due to the nature of its cubic lattice structure. During field emission, the electric field is concentrated at geometrically protrusive sites such as the four tip corners and the adsorbed contaminant molecules. The contaminant molecules keep rotating, migrating, and changing morphologies on the electron-emitting surface. This type of molecular movement causes the emission sites to change frequently in location. The emitted electrons can be visualized in the FEM pattern on the phosphorus screen after intensified by the MCP with a certain multiplication factor. The instability of electron emission can be directly observed by the appearing/disappearing of random bright spots in the FEM pattern. When the emitter is operated in

DOI: 10.1021/nl101752z | *Nano Lett.* **2010,** *10,* 3539–3544

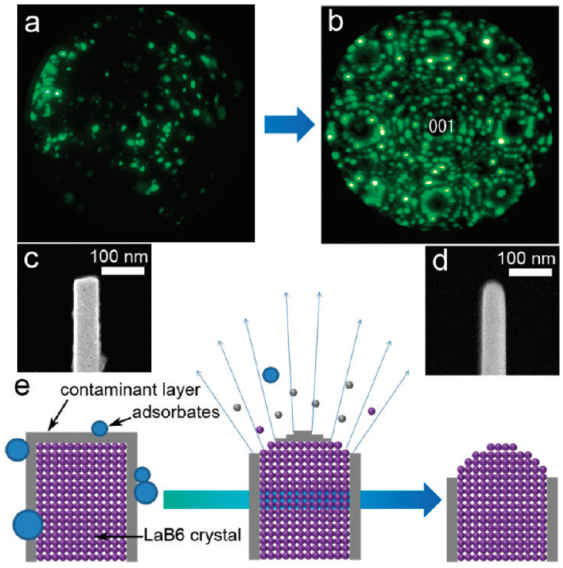

FIGURE 2. Process of field evaporation to obtain a clean hemispherical tip of a LaB_6 nanowire. (a) Disordered FIM pattern of the LaB_6 nanowire before field evaporation. (b) Crystallographically symmetric FIM pattern of the same LaB_6 nanowire after clean surface is obtained by field evaporation. (c) A typical SEM image of the LaB_6 nanowire tip before field evaporation. (d) SEM image of the same nanowire tip after field evaporation. (e) Schematic illustrations showing changes of the LaB_6 nanowire tip during the process of field evaporation, where adsorbates, contaminant layer, and LaB_6 crystal protrusions are removed under the application of a strong positive electric field.

the FIM mode, the imaging gases are ionized at the protrusive surface sites. When these ions reach the MCP, the generated signals are also intensified and visualized in the FIM pattern on the phosphorus screen. At this stage, the irregularities on the emitter surface would lead to a disordered FIM pattern as shown in Figure 2a. The central part of the pattern, which corresponds to the apex of the nanowire, remains dark compared to its surroundings, which correspond to corners and edges. As we further increased the applied voltage, it was observed that the initially dark apical region started to brighten and that the initially disordered FIM pattern would transform into an ordered one with a 4-fold symmetry, as shown in Figure 2b. This symmetric pattern agrees with the ⟨001⟩ projection stereograph of the LaB_6 crystal, which has a simple cubic lattice with space group $Pm3m$.[33] Two typical SEM images of the same LaB_6 nanowire tip before and after field evaporation are shown in Figure 2 panels c and d, respectively. By comparing these two images, two changes are observed. First, the originally flat tip has been modified into a smooth hemisphere. Second, some contaminant clusters attached on the nanowire surface have been removed by field desorption. These phenomena suggest that the structure had undergone a field evaporation process, which is illustrated schematically in Figure 2e. When a positive voltage is applied to the nanowire emitter, the strongest electric field is usually concentrated at the outmost contaminant layer and adsorbates due to their protrusive morphology. Since the binding between these contaminants and the LaB_6 nanowire is mostly of the nature of van der Waals interactions, it is much weaker compared to the strong covalent bonding within the LaB_6 crystal. The contaminants are therefore ionized and desorbed from the nanowire tip first. The FIM pattern at this stage is composed of large unstable bright spots due to the large clusters of contaminants. After the outmost contaminant layer is removed, a clean LaB_6 crystal is exposed to the electric field. The LaB_6 crystal at the corners was then also ionized and field-evaporated because of the concentrated local electric field. The FIM pattern at this stage usually has a dark central region surrounded by bright ordered spots of smaller size, which correspond to single La/B surface atoms. The slow field evaporation rate of the LaB_6 crystal allows the imaging gas to reach sufficient accommodation to give a bright FIM pattern with atomic resolution. When the voltage is further increased, the corners and edges of the LaB_6 crystal are gradually removed by field evaporation and the electric field over the entire tip reaches an equilibrium. A clean LaB_6 crystal surface with a smooth hemispherical geometry was then obtained. At this stage, the FIM pattern has a distribution of even brightness and individual surface La/B atoms can be resolved, as the one shown in Figure 2b.

A crystallographic indexation of such a clean FIM pattern is shown in Figure 3a. The pattern is indexed with the ⟨001⟩ projection stereograph of a simple cubic lattice. Besides the low index planes such as {100}, {110}, and {111}, high index planes of the type {210}, {211} and {221} have also developed into poles on the tip surface, which are resolved as concentric rings in the FIM pattern. The activation energy for field evaporation can be described as

$$Q_0 = \Lambda + I - \phi \tag{4}$$

where Λ is the sublimation energy of emitter material, I is the ionization energy, and ϕ is the surface work function.[25] Since the emitter work function ϕ varies for different crystal planes, field evaporation is usually orientation-dependent. Therefore facets on a nanowire tip due to field evaporation are expected to have different local radius of curvature around different crystal planes. A plane of higher work function usually has a larger radius of curvature due to deeper field evaporation. The variations in local radius of curvature will result in differences in the electric field distributed over the emitter tip. Variations of brightness in an FIM pattern are because the rate of ionization of the imaging gas only depends on the strength of the local electric field, assuming a uniform imaging gas accommodation rate over the entire emitter tip. However, in the case of a LaB_6 nanowire emitter, it is noticed that the FIM pattern has a rather uniform brightness, suggesting a uniform radius of curvature over the entire emitter tip. This is probably because the reactive imaging gas H_2 used in this study etched the LaB_6 crystal independent of orientation.[34] The measured

DOI: 10.1021/nl101752z | *Nano Lett.* **2010,** *10,* 3539–3544

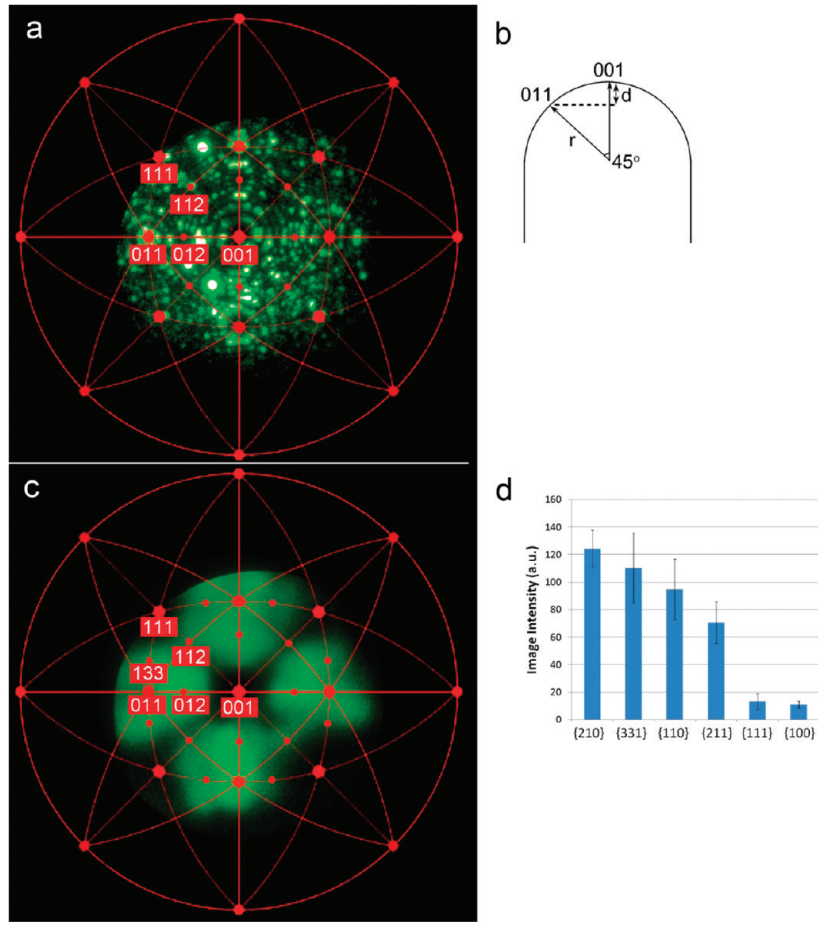

FIGURE 3. FIM and FEM pattern obtained from the clean surface of a ⟨001⟩ oriented LaB_6 single nanowire emitter. (A) FIM pattern obtained from the clean surface of the LaB_6 nanowire, where each pole is indexed according to the ⟨001⟩ projection stereograph of a simple cubic lattice. (B) Tip profile of the nanowire after field evaporation. (C) FEM pattern from the clean surface of the same nanowire, where the emission planes are also indicated. (D) Relative intensity of electron emission from {210}, {331}, {110}, {211}, {111}, and {100} planes.

screen distance between the first and the second ring about the ⟨001⟩ pole is 4.1 mm. This gives an image magnification of around 1 million knowing the LaB_6 {100} lattice spacing to be 4.15 Å. There are altogether 12 rings separating the center of the ⟨001⟩ pole and the center of the ⟨011⟩ pole. On the basis of the tip profile illustrated in Figure 3b, we can deduce the vertical distance d in the drawing as $d = 12 \times 4.15$ Å $= 5$ nm. The tip radius of curvature r equals $2d/(2 - 2^{1/2})$, which in turn gives a value of 17 nm. This value is smaller than 25 nm, which is half of the nanowire diameter. The tapering effect is believed to be caused by a preferential field etching on the peripheral of the emitter by the impurities in the imaging gas.[35] Such tapering was later confirmed by SEM observations. After recording the FIM patterns, we changed the system into field emission mode after a UHV environment of 10^{-9} Torr was restored. Figure 3c is an FEM pattern of the same nanowire emitter. The FEM pattern of the LaB_6 nanowire also shows a 4-fold symmetry. The brightness distribution in an FEM pattern is determined by the following two factors: (i) local electric field strength and (ii) work function. It is known from the uniformity in brightness in the FIM pattern that the electric field is distributed evenly over the entire tip apex. Therefore, the brightness in the FEM pattern only reflects the variations in the work function of different facets. From Figure 3c, it is noticed that the {210} and {331} planes have the brightest emission intensities and therefore they have the lowest work function. The {110} plane gives the second brightest emission intensity and followed by the {211} planes. The {100} and {111} planes are relatively low in emission intensity, and therefore they are expected to have higher work functions. The FEM intensities measured at each emission spot are given in Figure 3d. The sequence of work functions of the LaB_6 nanowire tip measured by FEM is as follows: {210, 331} < {110} < {211} < {100, 111}. It should be noted that this sequence is in some part different from those reported in the literature.[11−14] In most of the measurements reported in the literature, the clean surfaces of LaB_6 samples were obtained by heat-flashing. However, it has been recognized that heat-flashing changes inevitably surface composition and surface morphology of the treated material. We believe that the differences in the sequence of work functions between this work and others are largely due to differences in surface cleaning procedures.

DOI: 10.1021/nl101752z | *Nano Lett.* **2010,** *10,* 3539–3544

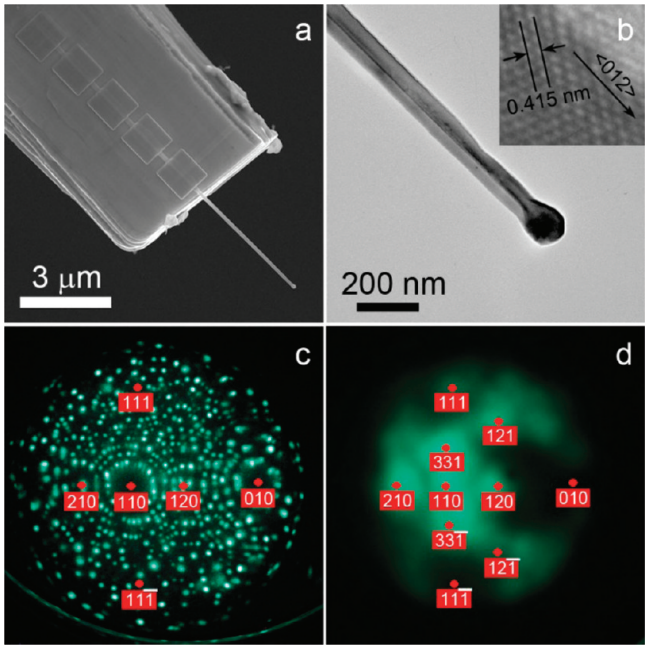

FIGURE 4. TEM, FIM, and FEM characterization of a ⟨012⟩-oriented LaB_6 single nanowire emitter. (a) SEM image of the nanowire emitter bonded to a W needle. (b) TEM image of the LaB_6 nanowire after field evaporation showing a nanowire diameter of around 100 nm. The inset is a high-resolution TEM image of a side of the nanowire showing its axial direction of ⟨012⟩. (c) FIM pattern of the same LaB_6 nanowire with indexed poles. (d) FEM pattern of the same LaB_6 nanowire, where {120} emission appears at the center of the pattern with highest intensity.

In some applications, it is technologically convenient to use a field emitter that has its lowest work function plane situated at the emitter apex. To demonstrate the possibility of making a LaB_6 nanowire emitter of such kind, we fabricated another emitter with a ⟨012⟩ oriented LaB_6 nanowire. Figure 4a is an SEM image of the fabricated emitter tip showing the fixed single LaB_6 nanowire and its supporting W base. Figure 4b is a TEM image of the nanowire tip after FIM and FEM studies. The nanowire is about 100 nm in diameter and its tip is of hemispherical geometry, which is due to field evaporation. From the high-resolution TEM (HRTEM) image presented in the inset of Figure 4b, we can identify the LaB_6 crystal structure with a lattice constant of 4.15 Å. The axis of the nanowire is oriented along the ⟨012⟩ lattice direction. Figure 4c is an FIM pattern of the same nanowire. It is noted that the ⟨012⟩ pole is situated at the center of the pattern, which agrees with the ⟨012⟩ nanowire orientation determined through HRTEM. Again, the uniformity in brightness of the FIM image intensities indicates that the nanowire tip is of smooth hemispherical geometry and the electric field is distributed evenly over the nanowire tip. Through a similar calculation, we obtained a tip radius of curvature value of 40 nm for this ⟨012⟩ oriented nanowire emitter, which is also slightly smaller than the half width of the nanowire. Figure 4d is an FEM pattern of the same nanowire tip. It is noted that the sequence in the FEM brightness is still the same as shown in the ⟨001⟩ oriented LaB_6 nanowire emitter: {210, 331} > {110} > {221} > {100, 111}. Again, it demonstrates that the FEM image brightness just reflects the distribution of work function of the various facets of the emitter tip.

The clean surface of LaB_6 nanowires obtained via field evaporation is also very stable. For a W CFE, it is known that after the initial flashing the field emission current usually undergoes a dramatic decay to below 10% of its initial emission current in a time span of just a few minutes. The changes of emitting surface can be directly visualized from the changes in an FEM pattern. In contrast, after field evaporation we did not observe any noticeable change in the FEM patterns for the LaB_6 nanowire emitter for a testing period extended to even a few hours. In addition, the emission current measurement showed no appreciable decay in emission current. The stability of the LaB_6 nanowire emitter surface cleaned by field evaporation is also significantly different from the LaB_6 needle emitter surface cleaned by heat-flashing. In the case of a LaB_6 needle emitter, crystallographically symmetrical FEM patterns can only last for a few minutes before losing its symmetry entirely after surface cleaning. Though heat-flashing was proven effective in obtaining a clean and stable surface in the case of a W emitter, it might not be a good choice for compound emitters. High-temperature heating can induce various types of unexpected changes at the surface, such as surface reconstruction, surface reactions with residual gases, and diffusion of impurities to the surface through the bulk.

The advantage of using field evaporation for a nanostructured compound emitter is clearly demonstrated here. The field evaporation process to a nanowire emitter is analogous to sharpening a pencil after each use. Since field evaporation at each time will remove at most materials of one or two nanometers in thickness, the micrometer-long nanowire can be cleaned in a repetitive manner. We believe that the cleaning process described here should be a versatile approach to obtain stable clean surface from a nanostructured emitter.

Though the {100} crystal plane does not exhibit the lowest work function, it is more stable thermodynamically and it has the highest crystallographic symmetry among all crystal planes.[36] Therefore, the ⟨001⟩ oriented LaB_6 nanostructured emitter is expected to provide the best stability and reliability when operated as a practical field emitter. On the other hand, the {210} plane has the lowest work function and therefore promises the highest field emission intensity and the lowest emission energy spread. The ⟨210⟩-oriented LaB_6 nanostructured field emitter should become the choice of use when a high-performance field electron emission source is desired.

Experimental Section. The single crystalline LaB_6 nanowires used in this study were synthesized using a chemical vapor deposition process based on a procedure that has already been published.[27] The pickup and alignment of a single LaB_6 nanowire were carried out using a home-built

DOI: 10.1021/nl101752z | *Nano Lett.* **2010,** *10,* 3539–3544

3D nanomanipulator. The W support needle used to attach a nanwire was modified to have a flat on its tip by focused ion beam (FIB) milling. After the single nanowire attachment, the W needle was transferred into a FIB + SEM dual beam system where electron-beam induced C deposition was carried out to make the C bonding pads. FIM and FEM studies were carried out using a dedicated UHV field emission measurement system. The FIM and FEM for the ⟨001⟩-oriented LaB_6 nanowire emitter was carried out at the liquid nitrogen temperature of 77 K. The extraction voltages for the FIM and FEM are 3 kV and −500 V, respectively. FIM was performed in a hydrogen gas pressure of 10^{-5} Torr and FEM was performed in a vacuum of 10^{-9} Torr. For the ⟨012⟩-oriented nanowire emitter, FIM and FEM were performed at a temperature of 40 K. The extraction voltages for the FIM and FEM are 6 kV and −900 V, respectively. FIM was carried under a He + 25% H_2 gas pressure of 8×10^{-6} Torr, and FEM was carried under a vacuum better than 10^{-9} Torr.

Acknowledgment. This work was partially supported by the Development of System and Technology for Advanced Measurement and Analysis, Japan Science and Technology Corporation (JST) and the Nanotechnology Network Project of the Ministry of Education, Culture, Sports, Science, and Technology (MEXT), Japan.

REFERENCES AND NOTES

(1) Schwind, G. A.; Magera, G.; Swanson, L. W. Comparison of parameters for schottky and cold field emission sources. *J. Vac. Sci. Technol., B* **2006**, *24*, 2897.
(2) Fowler, R. H.; Nordheim, L. Electron emission in intense electric fields. *Proc. R. Soc. London* **1928**, *119*, 173.
(3) Forbes, R. G. Physics of generalized Fowler-Nordheim-type equations. *J. Vac. Sci. Technol., B* **2008**, *26*, 788.
(4) Swanson, L. W.; Schwind, G. A. A Review of the Cold-Field Electron Cathode. *Adv. Imaging Electron Phys.* **2009**, *159*, 63.
(5) Kagarice, K. J.; Magera, G. G.; Pollard, S. D.; Mackie, W. A. Cold field emission from HfC(310). *J. Vac. Sci. Technol., B* **2008**, *26*, 868.
(6) Martin, E. E.; Trolan, J. K.; Dyke, W. P. Stable, high density field emission cold cathode. *J. Appl. Phys.* **1960**, *31*, 782.
(7) Ashihara, K.; Nakane, H.; Adachi, H. Experimental study of field emission characteristics as a function of the emitter to anode distance. *J. Vac. Sci. Technol., B* **1998**, *16*, 1180.
(8) Lafferty, J. M. Boride cathodes. *J. Appl. Phys.* **1951**, *22*, 299.
(9) Zaima, S.; Adachi, H.; Shibata, Y. Promising cathode materials for high brightness electron beams. *J. Vac. Sci. Technol., B* **1984**, *2*, 73.
(10) Adachi, H. Approach to a stable field emission electron source. *Scanning Electron Microsc.* **1985**, *2*, 473.
(11) Gesley, M.; Swanson, L. W. A determination of the low work function planes of LaB_6. *Surf. Sci.* **1984**, *146*, 583.
(12) Nishitani, R.; Aono, M.; Tanaka, T.; Oshima, C.; Kawai, S.; Iwasaki, H.; Nakamura, S. Surface structures and work functions of the LaB_6 (100), (110) and (111) clean surfaces. *Surf. Sci.* **1980**, *93*, 535.
(13) Oshima, C.; Aono, M.; Tanaka, T.; Kawai, S.; Shimizu, R.; Hagiwara, H. Thermionic emission from single crystal LaB_6 tips with [100], [110], [111], and [210] orientations. *J. Appl. Phys.* **1980**, *51*, 1201.
(14) Oshima, C.; Aono, M.; Tanaka, T.; Nishitani, R.; Kawai, S. Low work function and surface structure of the LaB_6 (210) surface studied by angle-resolved x-ray spectroscopy, ultraviolet spectroscopy, and low-energy electron diffraction. *J. Appl. Phys.* **1980**, *51*, 997.
(15) Zhang, H.; Tang, J.; Zhang, L.; An, B.; Qin, L.-C. Atomic force microscopy measurement of the young's modulus and hardness of single LaB_6 nanowires. *Appl. Phys. Lett.* **2008**, *92*, 173121.
(16) Futamoto, M.; Aita, T.; Kawabe, U. Microhardness of hexaboride single crystals. *Mater. Res. Bull.* **1979**, *14*, 1329.
(17) Morozov, W.; Malnev, V. I.; Dub, S. N.; Loboda, P. I.; Kresanov, V. S. Microhardness of LaB_6 single crystals and their resistance to ion bombardment. *Inorg. Mater.* **1984**, *20*, 1225.
(18) Windsor, E. E. Construction and performance of practical field emitters from lanthanum hexaboride. *Proc. IEEE* **1969**, *116*, 348.
(19) Futamoto, M.; Hosoki, S.; Okano, H.; Kawabe, U. Field emission and field ion microscopy of lanthanum hexaboride. *J. Appl. Phys.* **1977**, *48*, 3541.
(20) Nagata, H.; Harada, K.; Shimizu, R. Thermal field emission observation of single crystal LaB_6. *J. Appl. Phys.* **1990**, *68*, 3614.
(21) Nakamoto, M.; Fukuda, K. Field electron emission from LaB_6 and TiN emitter arrays fabricated by transfer mold technique. *Appl. Surf. Sci.* **2002**, *202*, 289.
(22) Qi, K. C.; Lin, Z. L.; Chen, W. B.; Cao, G. C.; Cheng, J. B.; Sun, X. W. Formation of extremely high current density LaB_6 field emission arrays via e-beam deposition. *Appl. Phys. Lett.* **2008**, *93*, No. 093503.
(23) Shimizu, R.; Kataoka, Y.; Kawai, S.; Tanaka, T. LaB_6 single crystal tips as an electron source of high brightness. *Appl. Phys. Lett.* **1975**, *27*, 113.
(24) Aida, T.; Futamoto, M.; Kawabe, U. Chemical and electrolytic reaction between LaB6 rods and HNO_3 aqueous solution. *Jpn. J. Appl. Phys.* **1979**, *18*, 1393.
(25) Nakamura, S. Field evaporation of metals in field ion microscope. *J. Electron Microsc.* **1966**, *15*, 279.
(26) Zhang, H.; Zhang, Q.; Tang, J.; Qin, L.-C. Single crystalline LaB_6 nanowires. *J. Am. Chem. Soc.* **2005**, *127*, 2862.
(27) Zhang, H.; Tang, J.; Zhang, Q.; Zhao, G. P.; Yang, G.; Zhang, J.; Zhou, O.; Qin, L.-C. Field emission of electrons from single LaB_6 nanowires. *Adv. Mater.* **2006**, *18*, 87.
(28) Hren, J. J.; Ranganathan, S. *Field ion microscopy*; Plenum Press: New York, 1968.
(29) Yeong, K. S.; Thong, J. T. L. Life cycle of a tungsten cold field emitter. *J. Appl. Phys.* **2006**, *99*, 104903.
(30) Wei, W.; Jiang, K. L.; Wei, Y.; Liu, P.; Liu, K.; Zhang, L. N.; Li, Q. Q.; Fan, S. S. LaB_6 tip-modified multiwalled carbon nanotubes as high quality field emission electron source. *Appl. Phys. Lett.* **2006**, *89*, 203112.
(31) Late, D. J.; More, M. A.; Misra, P.; Singh, B. N.; Kukreja, L. M.; Joag, D. S. Field emission studies of pulsed laser deposited LaB_6 films on W and Re. *Ultramicroscopy* **2007**, *107*, 825.
(32) Xu, J. Q.; Zhao, Y. M.; Zhang, Q. Y. Enhanced electron field emission from single crystalline LaB_6 nanowires with ambient temperature. *J. Appl. Phys.* **2008**, *104*, 124306.
(33) Futamoto, M.; Kawabe, U. Field ion microscopy of rare-earth hexaborides. *Surf. Sci.* **1980**, *93*, L117.
(34) Muller, E. W.; Nakamura, S.; Nishikawa, O.; McLane, S. B. Gas surface interactions and field ion microscopy of nonrefractory metals. *J. Appl. Phys.* **1965**, *36*, 2496.
(35) Rezeq, M. Tungsten nanotip fabrication by spatially controlled field assisted reaction with nitrogen. *J. Chem. Phys.* **2006**, *124*, 204716.
(36) Swanson, L. W.; Gesley, M. A.; Davis, P. R. Crystallographic dependence of the work function and volatility of LaB_6. *Surf. Sci.* **1981**, *107*, 263.

DOI: 10.1021/nl101752z | *Nano Lett.* **2010,** *10,* 3539--3544